

# Photoinduced Dissociation of Halobenzenes: Nonadiabatic Molecular Dynamics Simulations Reveal Key Pathways

Donghwan Im, Alekos Segalina,\* and Hyotcherl Ihee\*



Cite This: *J. Phys. Chem. Lett.* 2025, 16, 5228–5235



Read Online

ACCESS |



Metrics & More

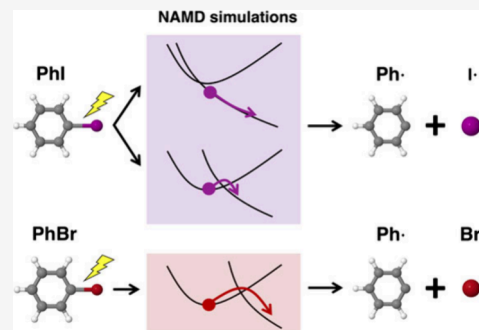


Article Recommendations



Supporting Information

**ABSTRACT:** Aryl halides are prototypical molecules for studying photodissociation, yet the role of spin–orbit coupling (SOC) in their dynamics remains incompletely understood. Using state-of-the-art *ab initio* calculations and excited-state dynamics simulations, we explore the photodissociation pathways of iodobenzene (PhI) and bromobenzene (PhBr). For PhI, two dissociation pathways, direct and indirect modes, are identified, consistent with gas-phase experiments. In contrast, photodissociation of PhBr occurs only after overcoming the energy barrier between bound and repulsive states, which requires activation of specific vibrational modes, particularly those associated with boat-like out-of-plane motion. While previous studies have suggested that SOC primarily accelerates intersystem crossing and photodissociation in heavier halogens, our results show that, in addition to SOC, the activation of specific vibrational modes also plays a crucial role in the dissociation process. These findings enhance our understanding of how SOC influences excited-state dynamics, providing insight into controlling photochemical reactivity in halogenated organic compounds.



In photochemistry, a detailed understanding of electronic state transitions is crucial for elucidating excited-state dynamics, which govern molecular behavior and reactivity in photoinduced processes.<sup>1–7</sup> Among the key processes governing excited-state dynamics are nonradiative transitions, which occur without the emission of light. These transitions fall into two main categories: internal conversion (IC), where energy dissipates within the same spin-states manifold, and intersystem crossing (ISC), which involves a spin-state change driven by spin–orbit coupling (SOC). In nonrelativistic quantum mechanics, ISC is spin-forbidden due to selection rules, whereas IC, mediated by nonadiabatic couplings (NACs), remains allowed. Nevertheless, ISC plays a crucial role in molecular photodynamics, governing processes such as phosphorescence and delayed fluorescence. It also plays a critical role in shaping solar energy conversion efficiency and photocatalytic processes.<sup>8,9</sup> Generally, when a molecule contains a heavy atom, the ISC rates increase due to the stronger SOC. In organometallic chemistry, this effect is deliberately exploited by incorporating heavy atoms into photocatalysts to enhance ISC efficiency, thereby prolonging triplet-state lifetimes.<sup>10–12</sup> The effect of SOC is critical not only in heavy metal complexes but also in small organic molecules for photophysical processes. For example, metal-free emitters in phosphorescent organic light-emitting diodes (PhOLEDs) designed with flexible molecular structures and atoms possessing lone-pair electrons, such as nitrogen, oxygen, or sulfur, can readily undergo ISC, boosting the triplet population.<sup>13–18</sup>

Aryl halides have long served as model molecules for studying photodissociation processes.<sup>19–39</sup> Numerous time-resolved experiments in both gas and solution phases have shown that the photodissociation rate of aryl halides increases with the mass of the halogen atom. According to research by Kadi et al., the carbon–halogen (C–X, where X represents the halogen atom) bond dissociation dynamics in aryl halides are strongly influenced by the halogen’s atomic mass.<sup>32</sup> Specifically, the reported time constants for photodissociation are less than 1 ps for iodobenzene (PhI), 28 ps for bromobenzene (PhBr), and 1 ns for chlorobenzene (PhCl), entailing the dissociation rate trend: I > Br > Cl. These studies have widely explored the possibility that these variations stem from the specific nature of the excited states involved in photodissociation. In PhI, photodissociation has been proposed to proceed via two distinct pathways: direct-mode and indirect (complex-mode) dissociation. Employing kinetic-energy-resolved time-of-flight (KETOF) mass spectrometry, Cheng et al. investigated these pathways and identified a direct-mode dissociation with a time constant of approximately 400 fs, while complex-mode dissociation occurred more slowly, with a time constant of approximately 600 fs.<sup>27</sup> Similarly, Kadi et al.,

**Received:** February 28, 2025

**Revised:** March 30, 2025

**Accepted:** April 14, 2025

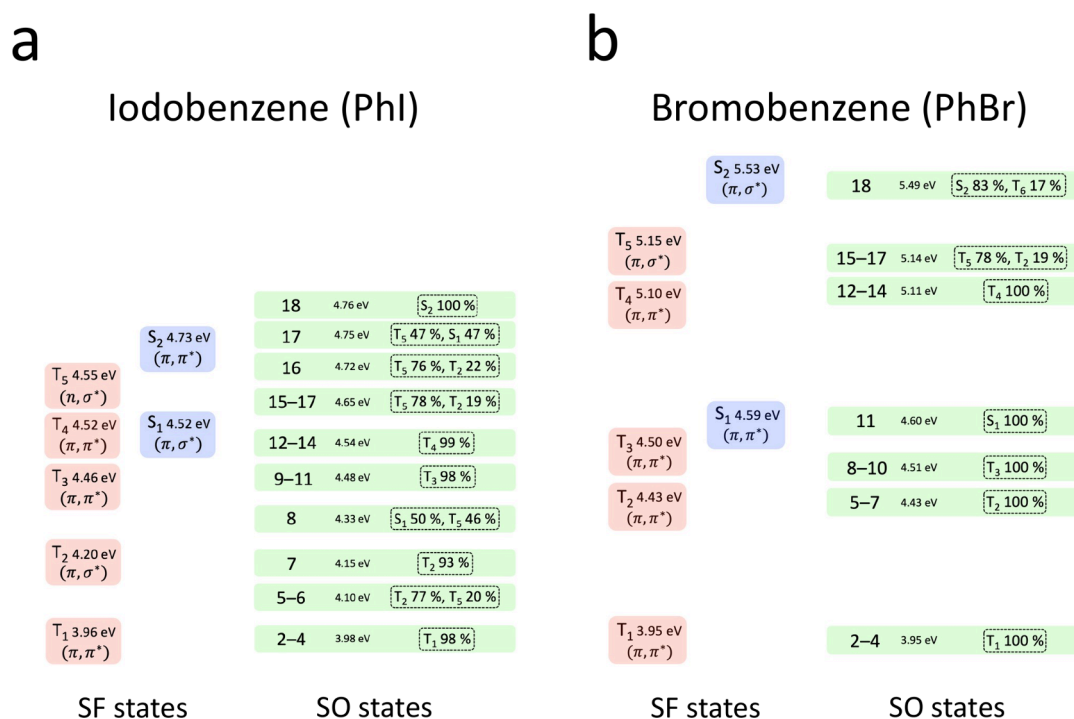


**Figure 1.** Nature of the excited states in the A-band region for PhI and PhBr is shown in panels (a) and (b), respectively. On the left, the SF states are labeled with their energy levels and electronic transition characters. On the right, the electronic energy levels of SO states and the contributions of SF states to them are provided. For the nomenclature of SO states, we number the states starting from the lowest electronic state. Triplet SF states are colored red, and SF singlet states are colored blue.

employing similar techniques, reported two dissociation time constants, 350 and 700 fs, which were attributed to two distinct pathways.<sup>32</sup>

Employing multistate second-order complete active space perturbation theory (MS-CASPT2), Liu et al. attributed the dissociation of PhBr and PhCl to strong spin–orbit coupling (SOC), which facilitates curve crossings between the bound  $S_1$  state and repulsive triplet states.<sup>28</sup> Additionally, they identified two distinct dissociation pathways for PhI: one arising from the direct dissociation of the  $S_1$  ( $n, \sigma^*$ ) state and the other proceeding via ISC from the bound  $S_2$  ( $\pi, \pi^*$ ) state to the repulsive  $T_2$  and  $T_5$  states, which exhibit ( $n, \sigma^*$ ) character. Recently, using Ehrenfest dynamics simulations, Scheiner et al. reported that all dissociation pathways of PhI appear to be accessible through nonadiabatic and nonradiative transitions.<sup>21</sup> While these theoretical studies have provided valuable mechanistic insights, the detailed dynamical aspects of these dissociation pathways, the exact role of SOC in facilitating ISC and photodissociation remains elusive. This underscores the need for computational studies that incorporate SOC effects in a dynamical fashion to fully understand their role in the photodissociation processes of aryl halides.

In an effort to bridge the gap in understanding the role of SOC in the photodissociation of aryl-halides, we employed state-of-the-art *ab initio* calculations and nonadiabatic molecular dynamics (NAMD) simulations, within the surface hopping framework, for PhI and PhBr. Previous theoretical studies have been limited by the challenges of accurately incorporating SOC and nonadiabatic effects within a fully dynamic framework. These calculations are computationally highly demanding due to strong electronic state mixing, requiring the simultaneous consideration of multiple state couplings. In this contribution, we first analyzed the electronic

structures of aryl halides using high-accuracy multireference static calculations. Based on the selected computational framework, we hence performed NAMD simulations incorporating SOC effects, enabling ISC events, to investigate the photodissociation processes in PhI and PhBr. This allows us to explore the role of both SOC and vibronic effects in the photodissociation dynamics. Details of our calculations are provided in the [Computational Details](#) section.

Initially, we focus on the characterization of the excited states manifold of PhI and PhBr. Since numerous experimental studies have been conducted following excitation in the weak A-band, which spans wavelengths between 240 and 320 nm, our goal was to investigate the excited states within this energy range. [Figure 1](#) presents the electronic energy levels and illustrates the character of the excited states for PhI and PhBr in both spin-free (SF) and spin–orbit (SO) representations. Shortly, in the SF representation, electronic states are described as spin-pure singlets or triplets, whereas SO representation characterizes electronic states as combinations of SF states. Therefore, SO representation can account for state mixing induced by SOC, making it particularly advantageous for describing highly coupled states, as in systems incorporating heavy atoms like iodine. For both PhBr and PhI, numerous electronic states are located in the A-band region, including bound states having ( $\pi, \pi^*$ ) character and repulsive states exhibiting either ( $n, \sigma^*$ ) or ( $\pi, \sigma^*$ ) character. In the case of PhI, electronic states having bound and repulsive characters are both accessible upon photoexcitation in the A-band. Among the electronic states of PhI in the A-band region, SO state 8 (see [Figure 1](#) and [Table S1](#) for reference) exhibits the largest oscillator strength. SO State 8 features a spin–orbit-coupled nature, combining the  $S_1$  SF state with ( $\pi, \sigma^*$ ) character and the  $T_5$  SF state with ( $n, \sigma^*$ ) character. This result

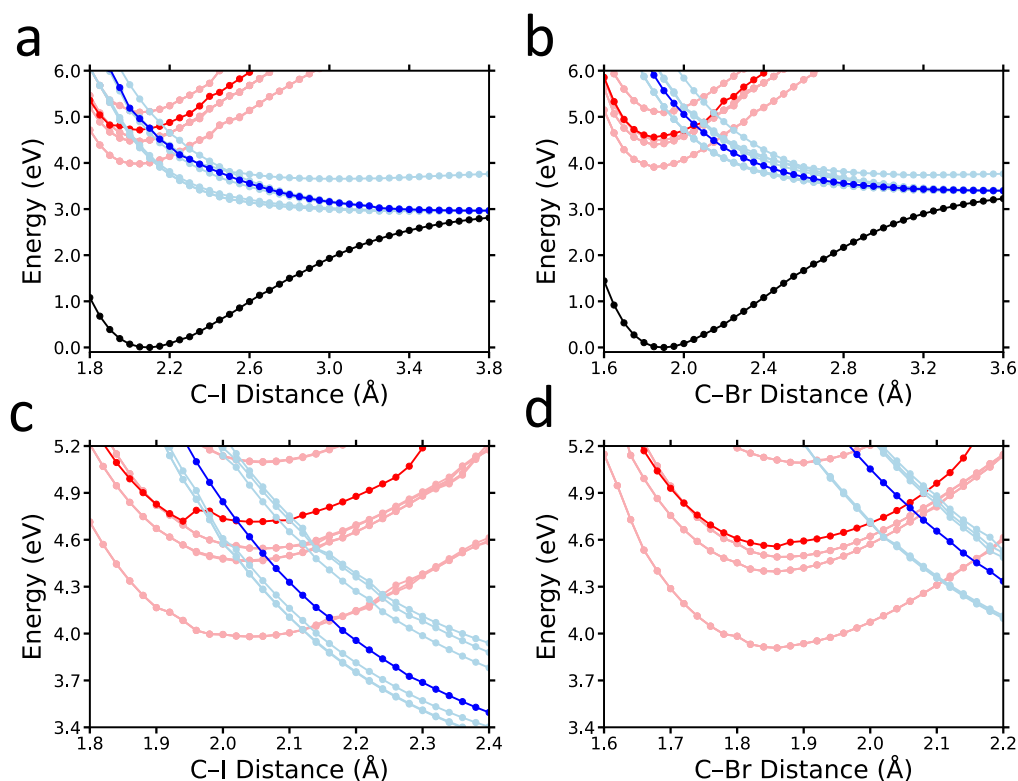


**Figure 2.** One-dimensional semidiabatic PECs of SO states for PhI (a, c) and PhBr (b, d). Semidiabatization was performed by analyzing orbital occupation numbers and the contributions of SF states to SO states, based on adiabatic PECs. The PECs are divided into two groups: bound and repulsive states, as well as those with predominantly singlet or triplet characters. Bound states are shown in red, while repulsive states are depicted in blue. Solid colors indicate states with primarily singlet characters, whereas fainter colors represent states with mostly triplet characters. Panels c and d provide a closer view of the PECs near the FC region, as depicted in panels a and b, respectively.

is consistent with the findings of Devarajan et al. and Sage et al., both of which report the presence of bright spin-orbit-coupled repulsive states within the A-band energy range.<sup>29,36</sup> The vertical excitation energy of SO State 8, which comprises approximately 50% of the  $S_1$  SF state and 46% of the  $T_5$  SF states, is approximately 0.2 eV lower than that of the uncoupled  $S_1$  and  $T_5$  SF states. This energy reduction highlights the significant influence of SOC in stabilizing this repulsive state within the Franck–Condon (FC) region. Not only SO state 8, but also several bound ( $\pi, \pi^*$ ) states that lie within the A-band region, such as SO states 7 and 18, exhibit significant oscillator strength. Consequently, it is feasible that excitation in the A-band can access both repulsive and bound states of PhI. Conversely, for PhBr, no repulsive states are accessible with A-band excitation. Based on the oscillator strength of the excited states of PhBr, the only electronic state accessible in the A-band is SO state 11, which predominantly exhibits a singlet ( $\pi, \pi^*$ ) character. We note that the SO states of PhBr in the A-band region exhibit nearly pure singlet or triplet character. Given the small norm of spin-orbit coupling matrix element (ISOCMEI) value of  $1.00 \text{ cm}^{-1}$  between the  $S_1$  and  $T_1$  states, and below  $0.1 \text{ cm}^{-1}$  between  $S_1-T_2$  and  $S_1-T_3$ , it is unlikely that SOC significantly alters the positions of the SO states compared to the SF states.

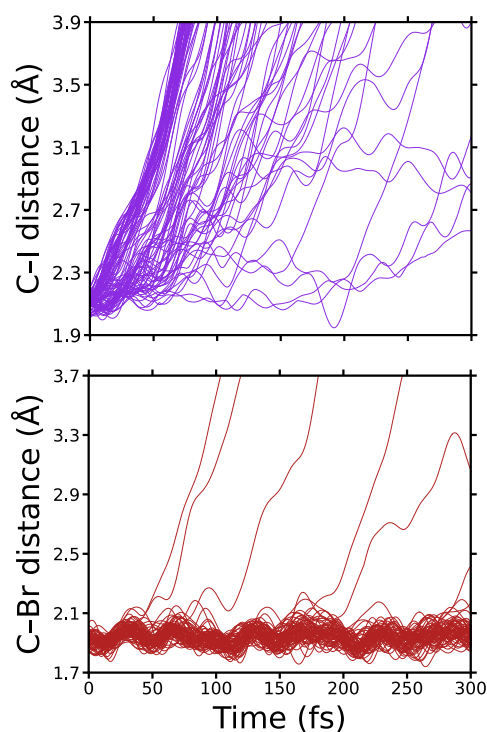
To identify the region of curve-crossing between bound and repulsive states, the potential energy curves (PECs) were computed as a function of the C–I and C–Br distances for PhI and PhBr, respectively. Based on the adiabatic PECs for the SO states shown in Figures S1–2, a semidiabatization procedure was performed, carefully considering the orbital and spin

characteristics of the excited states. Specifically, we identified and connected the SO states at consecutive points along the PECs, focusing on those with the most similar electronic configurations and spin states. This procedure allowed us to express the states in the diabatic picture, ensuring a smooth representation of the SO states along the PECs. This approach offers the advantage of clearly identifying regions of curve crossings, which is not as straightforward in adiabatic representation, especially in systems exhibiting large SOC. In Figure 2, the one-dimensional PECs for the semidiabatized SO states are presented for both PhBr and PhI. The PECs are calculated over the C–I distance range of 1.8 to 3.8 Å for PhI, and the C–Br distance range of 1.6 to 3.6 Å for PhBr. For PhI, the curve crossings turn out to be located near the FC region, particularly within the energy range of the A-band. This suggests that excitation to the bound SO state 7 or SO state 18 of PhI may lead to rapid photodissociation after state crossing, with little to no energy barrier. Conversely, for PhBr, the repulsive curves are shifted to higher energy levels, causing curve crossings to occur at longer C–Br bond distances. Thus, after excitation to SO state 11, an energy barrier of  $\sim 0.2 \text{ eV}$  must be overcome to reach the crossing point, significantly slowing the photodissociation of PhBr. To further investigate the influence of halogen atomic mass on curve-crossing locations, we analyzed the curve-crossing region of PhCl. As shown in Figure S3, the adiabatic PECs of PhCl reveal that the curve crossings occur at higher energies than PhBr. Our static calculations highlight the role of SOC in the dissociation of PhI and PhBr, as well as the influence of the energy barrier between repulsive and bound states, which depends on atomic

mass. However, several questions remain unresolved, particularly concerning the dynamical properties, such as the key nuclear motions of PhI and PhBr leading to the dissociation of the halogen atom.

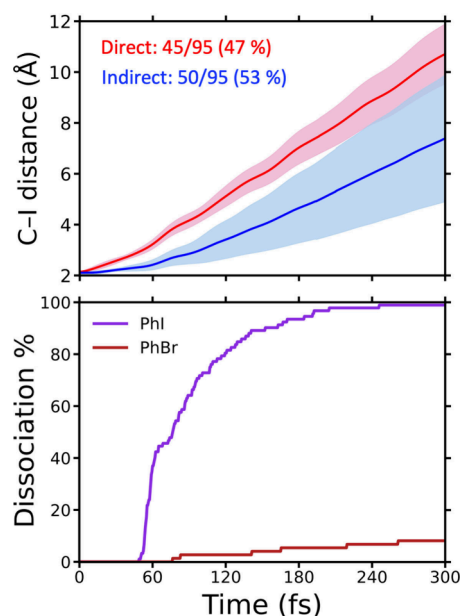
To gain deeper insight from a dynamics perspective, we conducted NAMD simulations to investigate the excited-state behavior of PhI and PhBr. NAMD simulations were performed using the Surface Hopping Including Arbitrary Couplings (SHARC) method, enabling the incorporation of SOC effects into the surface hopping framework.<sup>40,41</sup> Given the challenges of describing photodissociation processes with single-reference methods, such as time-dependent density functional theory (TD-DFT), here we employed the state-averaged complete active space self-consistent field (SA-CASSCF) method for electronic structure calculations. Simulations were initiated from the excited states within the energy range of 4.6 to 5.0 eV, corresponding to excitation in the A-band region, with a particular focus on 267 nm (4.64 eV) to match the wavelength used in previous experiments. This energy range was selected based on the calculated absorption spectra of each molecule, derived from the oscillator strengths obtained using geometries sampled from a harmonic Wigner distribution (Figure S4–5). The simulations were conducted up to 300 fs for PhI and 1 ps for PhBr.

Figure 3 shows the time evolution of the C–X (X = I; Br) bond distance for both molecules. Nearly all PhI trajectories



**Figure 3.** Time evolution of the C–I and C–Br bond distances is shown in the upper and lower panels, respectively, up to 300 fs.

exhibit rapid photodissociation within the first 300 fs, with a wide range of dissociation speeds. In contrast, fewer than 15% of the PhBr trajectories show comparable C–Br bond dissociation within 300 fs, as shown in the lower panel of Figure 4. As anticipated from static calculations, this difference in photodissociation yields primarily stems from the nature of the excited states accessed immediately after photoexcitation



**Figure 4.** Upper panel shows the time evolution of the C–I bond distance for two groups of trajectories: fast and slow dissociation. The solid lines represent the average bond distances, with the shaded regions indicating the  $1\sigma$  standard deviation for each group. The lower panel presents the percentage of C–X bond dissociation as a function of time. Dissociation is defined as occurring when the C–X bond length exceeds 1.5 times its equilibrium bond length. Nearly 100% of the trajectories for PhI exhibit dissociation within 300 fs, whereas fewer than 20% of PhBr trajectories dissociate within the same time frame. Dissociation is classified as “direct” if the C–I bond distance exceeds 2.5 Å within 40 fs; otherwise, it is categorized as “indirect”.

and the position of the curve crossings. For PhI, the rapid C–I bond dissociation is attributed to the large oscillator strength of the repulsive SO state 8 and the bound-repulsive crossing point coinciding near the FC region. In contrast, for PhBr, only bound states are accessible upon A-band excitation, and the energy barrier for crossing to the repulsive state results in relatively slower dissociation of the C–Br bond.

From the PhI trajectories, two distinct distributions of C–I distances emerge, particularly within the first 50 fs: (1) direct dissociation, marked by consistently high velocity, and (2) indirect dissociation, where the C–I bond undergoes a period of nondissociative motion before recoiling at a relatively lower velocity. We established a criterion to differentiate these pathways, defining a trajectory as following a direct dissociative pathway if the C–I bond length exceeds 2.5 Å within 40 fs, a qualitative measure derived from the trends observed in the Figure S6. Following this classification, we calculated the average bond lengths at each time step and their standard deviations, which are gathered in the upper panel of Figure 4. In our NAMD simulation, 47% of the trajectories exhibited rapid dissociation without significant C–I bond oscillation, while 53% showed relatively slower dissociation. The time-resolved populations of the two dissociation pathways are plotted in Figure S7. In the direct dissociation pathway, the initial population shows a mixed character of singlet and triplet states, with each comprising approximately 40%. This suggests that initial excitation may populate repulsive states, primarily SO state 8, which exhibits strong spin–orbit mixing. In contrast, the indirect dissociation initially populated predom-

inantly singlet states, with 80% of the trajectories in the singlet states manifold. However, due to the strong SOC between bound singlet states and repulsive triplet states, ultrafast ISC was observed, subsequently leading to photodissociation within 200 fs. Thus, it is confirmed that the SOC plays a significant role in both the direct and indirect pathways of PhI.

Additionally, we observed that the trajectories associated with direct dissociation showed a narrow distribution of C–I bond dissociation speeds, while those associated with indirect dissociation exhibited a broader range. This behavior provides insight into previous photofragment translational spectroscopy experiments, which observed both a sharp high-velocity component and a broad low-velocity component. From the NAMD simulations, we obtained recoil velocities of 0.028 Å/fs for the trajectories showing direct dissociation, and 0.017 Å/fs for trajectories showing indirect dissociation. These values are qualitatively consistent with experimental results, which report a recoil velocity of 0.021 Å/fs for trajectories exhibiting direct dissociation and approximately half that value for trajectories exhibiting indirect (complex) dissociation.<sup>27</sup> Considering the PECs of PhI, direct photodissociation is facilitated following the excitation of repulsive states, which concentrate energy in the C–I bond while minimizing redistribution to the phenyl ring. Conversely, excitation to bound states allows time for vibrational energy to dissipate not only in the C–I bond but also within the phenyl ring before transitioning to repulsive states, leading to indirect photodissociation and broader energy distribution due to the redistribution of energy across other degrees of freedom.

In the case of PhBr, less than 30% of trajectories show dissociation within 1 ps, as shown in the lower panel of Figure 4 and in the computed C–Br distance over the dynamics in Figure S8. Notably, ISC to the triplet state occurred much more slowly compared to PhI, as shown in Figure S9. For the 55 nondissociative trajectories for PhBr, we performed normal-mode analysis (NMA) to investigate the normal mode activity in the bound state, considering the harmonic frequencies of PhBr in  $S_1$  state, summarized in Table S5. The upper panel of Figure 5 shows the activity of normal mode ( $R_{act}$ ), calculated every 100 fs, while the lower panel provides a graphical representation of the analyzed vibrational modes. NMA revealed that the  $R_{act}$  of  $\nu_5$  mode, corresponding to C–Br bond stretching, remained high during the first 1 ps. The activity of the  $\nu_4$  mode, associated with the boat-like motion, gradually increased over time. This behavior appeared in phase with the initial high activity of in-plane phenyl ring motions, such as  $\nu_{10}$ ,  $\nu_{14}$ , and  $\nu_{16}$ , which diminished as the  $\nu_4$  mode became more dominant. This complementary evolution underscores an interplay between the boat-like out-of-plane motion and in-plane vibrations, reflecting a dynamic redistribution of vibrational energy. To investigate the role of this out-of-plane motion in the photodissociation of PhBr, single-point calculations were performed at the CASSCF level using geometries corresponding to  $Q = 0$  and  $Q = 1$ , which represent the variations along the  $\nu_4$  mode direction. Figure S10 shows the  $\pi^*$  and  $\sigma^*$  orbitals included in the active space for these geometries. Significant mixing of the  $\pi^*$  and  $\sigma^*$  orbitals is observed in the  $Q = 1$  geometry, whereas no such mixing occurs in the  $Q = 0$  geometry. Starting from the  $Q = 0$  and  $Q = 1$  geometries, we calculated 1D PECs and |SOCMEI| values along the C–Br coordinate, as reported in Table S6 and shown in Figure S11. In the  $Q = 0$  case, even near the crossing point between the  $^1(\pi, \pi^*)$  and  $^3(n, \sigma^*)$  states, the |SOCMEI|

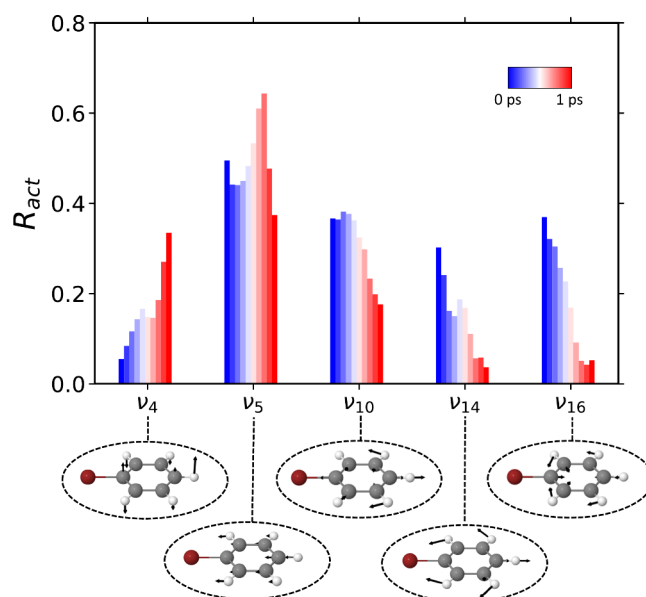


**Figure 5.** Results of NMA for PhBr. The value of  $R_{act}$  is presented over every 100 fs interval with the corresponding normal modes showing the intensity of  $R_{act}$  above 0.3 at any step in NAMD simulations. Notably, the NMA was conducted using the normal modes of PhBr in its bound  $S_1$  state.

values remain below  $2 \text{ cm}^{-1}$ , indicating a low probability of ISC. In contrast, when the  $\nu_4$  mode is activated ( $Q = 1$ ), the |SOCMEI| values increase significantly near the crossing point, exceeding those in the  $Q = 0$  case by more than a factor of 20. This is in line with a recent study, which showed that a drastic enhancement of SOC occurs near the crossing point between diabatic states.<sup>42</sup> Examining the trend of orbitals mixing with respect to the  $\nu_4$  normal mode vector, the vibrational energy transfer between the in-plane modes of PhBr and the  $\nu_4$  mode accelerates the curve crossing in conjunction with the consistently active  $\nu_5$  mode. These results align with the findings of Sobolewski et al., who reported that the coupling of the  $^1(\pi, \pi^*)$  state with the  $^1(\pi, \sigma^*)$  state is facilitated by the twisting motion of the aromatic ring.<sup>23</sup> As discussed in the NMA section of Supporting Information (SI), the  $R_{act}$  values may depend on the time step. Therefore, we calculated  $R_{act}$  using different time steps, and the results confirm that the calculated values are not significantly affected, as shown in Figure S12. Consequently, it is expected that curve crossing is induced by the activation of the boat-like out-of-plane  $\nu_4$  vibrational mode. This underscores how the activation of a symmetry-breaking out-of-plane vibrational mode can enhance SOC, playing a dominant role in ISC between bound and repulsive states.

This study investigates the photodissociation dynamics of PhI and PhBr using multireference electronic structure calculations and excited-state dynamics simulations, explicitly incorporating the effects of SOC. Our results reveal that the large SOC in PhI facilitates ultrafast photodissociation by enabling significant singlet–triplet mixing, which directly lowers the energy of repulsive states in the A-band region. Although excitation to the bound states can occur, the curve crossing near the FC region subsequently induces ultrafast curve crossing, leading to photodissociation. In contrast, for PhBr, where SOC is weaker, vibrational energy redistribution in the bound state plays a dominant role. In the A-band region,

direct access to the repulsive state is restricted. After excitation to the bound state, specific vibrational modes, such as the out-of-plane  $\nu_4$  mode, assist the system in overcoming energy barriers for curve crossing. However, the activation of slower vibrational modes takes time, subsequently slowing down the photodissociation of PhBr. This work highlights the complex interplay between SOC and vibronic effects in governing photochemical reactivity and demonstrates the importance of vibrational dynamics in systems with small SOC. A mechanistic understanding of the factors controlling photodissociation rates is provided by reconciling dynamic simulations with experimental observations. These findings offer new insights into the multidimensional nature of curve crossings, and the complex interplay between SOC and vibrational dynamics, laying the groundwork for future studies of excited-state processes in organic systems, particularly including those containing heavy atoms.

## COMPUTATIONAL DETAILS

The vertical excitation energies of the excited states of PhBr and PhI were calculated using extended multistate second-order complete active space perturbation theory (XMS-CASPT2),<sup>43,44</sup> and the results are summarized in Table S1–2. We employed ANO-RCC-VTZP basis set, a contracted version of the ANO-RCC basis set at the triple- $\zeta$  level.<sup>45</sup> The reference equilibrium ground-state geometries were optimized at the second-order Møller–Plesset perturbation theory (MP2) level with the ANO-RCC-VDZP basis set, chosen for their good agreement with experimental structures, as shown in Table S3–4. The reference wave function was computed using state-averaged complete active space self-consistent field (SA-CASSCF) calculations with a (12e, 10o) active space. The active space included  $\pi$  and  $\pi^*$  orbitals of the benzene ring,  $\sigma$  and  $\sigma^*$  orbitals of the C–I bond, and two nonbonding p orbitals localized on each iodine atom. A total of 12 singlet and 12 triplet states were incorporated in the state-averaging procedure for both PhI and PhBr. To mitigate the well-known intruder state problem in CASPT2 calculations, an imaginary shift of 0.25 au was applied,<sup>46</sup> without an IPEA shift. Relativistic effects were accounted for using the second-order Douglas-Kroll-Hess (DKH2) Hamiltonian.<sup>47</sup> Spin–orbit coupling matrix elements (SOCMEs) were computed using the RASSI module<sup>48</sup> in OpenMolcas software,<sup>49–51</sup> following the calculation of spin–orbit integrals with the atomic mean-field integral (AMFI) approach,<sup>52</sup> which approximates the spin–spin coupling contribution to the spin–orbit Hamiltonian. To limit the computational burden, the resolution-of-the-identity Cholesky decomposition (RICD) technique<sup>53</sup> was employed with an auxiliary basis set for the approximation of two-electron integrals. Potential energy curves (PECs) of PhI and PhBr were computed at the XMS-CASPT2/ANO-RCC-VTZP level as a function of the C–I or C–Br bond distance, respectively, with all other structural parameters constrained. To explore the dynamics of carbon–halogen bond dissociation dynamics in halobenzenes, trajectory surface hopping simulations were carried out for PhI and PhBr. For the initial condition, 1000 geometries were sampled using the Hessians obtained with the MP2/ANO-RCC-VDZP level of theory, with a 0 K harmonic Wigner distribution. Vertical excitation energies and oscillator strengths for the sampled geometries were calculated at the SA-CASSCF level of theory. Based on this information, initial conditions (ICs) were stochastically set based on the excitation energies and the oscillator strengths in

the energy range of 4.6 to 5.0 eV, corresponding to the pump energy employed in the previous gas-phase experiments. To treat IC and ISC on the same footing, NAMD simulations were performed using the SHARC formalism with SA-CASSCF/ANO-RCC-VDZP level of theory.<sup>40,41</sup> We note that the location of the crossing between bound and repulsive states is similar across excited states within the A-band region of the PECs, calculated with SA-CASSCF and XMS-CASPT2 levels of theory, as shown in Figure S13. This approach incorporates spin-state mixing effects induced by SOC into surface hopping simulations. Briefly, in the molecular Coulomb Hamiltonian, which is the standard Hamiltonian for most quantum chemistry calculations, the SO effect is incorporated through an additional approximate Hamiltonian, such as the mean-field approach that we previously employed for static calculations. After constructing and diagonalizing this effective Hamiltonian, the transition probabilities (or hopping probabilities) were determined by evaluating the coupling between the resulting eigenstates. During the simulations, a total of 19 SO states were active, consisting of 4 singlet and 5 triplet SF states. In order to ensure the stability of the CASSCF wave function during the NAMD simulations, we had to extend the number of states included in the state-averaging procedure, employing six singlet and six triplet states. Instead of calculating nonadiabatic coupling vectors, overlap matrices were calculated with a local diabaticization scheme<sup>54,55</sup> and propagated with a substep of 0.02 fs for the three-step wave function propagator. Normal mode analysis (NMA) was performed using the built-in module implemented in the SHARC package.<sup>56</sup> Using the Velocity Verlet algorithm, nuclei were propagated with the time step of 0.5 fs. The energy-based decoherence scheme, with a decoherence parameter of 0.1 hartree as recommended by Granucci and co-workers,<sup>57</sup> was employed to minimize the overcoherence problem in the surface hopping simulations.

## ASSOCIATED CONTENT

### Supporting Information

The Supporting Information is available free of charge at <https://pubs.acs.org/doi/10.1021/acs.jpcllett.5c00622>.

Brief description of NMA; Characteristics of excited state of PhI (Table S1) and PhBr (Table S2); geometrical parameters of PhI (Table S3) and PhBr (Table S4); harmonic frequencies of PhBr in  $S_1$  state (Table S5); ISOCMEI values of PhBr (Table S6); Adiabatic PECs of PhI (Figure S1), PhBr (Figure S2) and PhCl (Figure S3); the absorption cross-section spectrum of PhI (Figure S4) and PhBr (Figure S5); Individual trajectories of PhI (Figure S6) and state population (Figure S7); C–Br distance up to 1 ps (Figure S8); State population of PhBr (Figure S9); representative active space of PhBr in  $Q = 0$  and  $Q = 1$  (Figure S10); and 1D PECs along the  $Q = 0$  and  $Q = 1$  (Figure S11); activities of normal mode in 500 fs time step (Figure S12); 1D PECs of PhI and PhBr calculated with SA-CASSCF and XMS-CASPT2 level of theory (Figure S13) (PDF)

Transparent Peer Review report available (PDF)

## AUTHOR INFORMATION

## Corresponding Authors

**Alekos Segalina** – Center for Advanced Reaction Dynamics (CARD), Institute for Basic Science (IBS), Daejeon 34141, Republic of Korea; Department of Chemistry, Korea Advanced Institute of Science and Technology (KAIST), Daejeon 34141, Republic of Korea; [orcid.org/0000-0001-6600-554X](https://orcid.org/0000-0001-6600-554X); Email: [alekos@ibs.re.kr](mailto:alekos@ibs.re.kr)

**Hyocheol Ihee** – Center for Advanced Reaction Dynamics (CARD), Institute for Basic Science (IBS), Daejeon 34141, Republic of Korea; Department of Chemistry, Korea Advanced Institute of Science and Technology (KAIST), Daejeon 34141, Republic of Korea; [orcid.org/0000-0003-0397-5965](https://orcid.org/0000-0003-0397-5965); Email: [hyotcherl.ihee@kaist.ac.kr](mailto:hyotcherl.ihee@kaist.ac.kr)

## Author

**Donghwan Im** – Center for Advanced Reaction Dynamics (CARD), Institute for Basic Science (IBS), Daejeon 34141, Republic of Korea; Department of Chemistry, Korea Advanced Institute of Science and Technology (KAIST), Daejeon 34141, Republic of Korea; [orcid.org/0009-0002-2306-3701](https://orcid.org/0009-0002-2306-3701)

Complete contact information is available at:  
<https://pubs.acs.org/10.1021/acs.jpcllett.5c00622>

## Notes

The authors declare no competing financial interest.

## ACKNOWLEDGMENTS

This work was supported by the Institute for Basic Science (IBS-R033). We thank the IBS Research Solution Center (RSC) for supporting computational resources.

## REFERENCES

- (1) Lasorne, B.; Worth, G. A.; Robb, M. A. Excited-state Dynamics. *WIREs Comput. Mol. Sci.* **2011**, *1* (3), 460–475.
- (2) Tamai, N.; Miyasaka, H. Ultrafast Dynamics of Photochromic Systems. *Chem. Rev.* **2000**, *100* (5), 1875–1890.
- (3) Heo, J.; Kim, D.; Segalina, A.; Ki, H.; Ahn, D.-S.; Lee, S.; Kim, J.; Cha, Y.; Lee, K. W.; Yang, J.; Nunes, J. P. F.; Wang, X.; Ihee, H. Capturing the Generation and Structural Transformations of Molecular Ions. *Nature* **2024**, *625* (7996), 710–714.
- (4) Kim, S.; Ahn, D.-S.; Ahn, M.; Wee, K.-R.; Choi, J.; Ihee, H. Charge transfer induced by electronic state mixing in a symmetric X–Y–X-type multi-chromophore system. *Phys. Chem. Chem. Phys.* **2020**, *22* (48), 28440–28447.
- (5) Brinks, D.; Hildner, R.; Van Dijk, E. M. H. P.; Stefani, F. D.; Nieder, J. B.; Hernandez, J.; Van Hulst, N. F. Ultrafast dynamics of single molecules. *Chem. Soc. Rev.* **2014**, *43* (8), 2476–2491.
- (6) Ihee, H.; Lobastov, V. A.; Gomez, U. M.; Goodson, B. M.; Srinivasan, R.; Ruan, C.-Y.; Zewail, A. H. Direct Imaging of Transient Molecular Structures with Ultrafast Diffraction. *Science* **2001**, *291* (5503), 458–462.
- (7) Choi, E. H.; Lee, Y.; Heo, J.; Ihee, H. Reaction dynamics studied via femtosecond X-ray liquidography at X-ray free-electron lasers. *Chem. Sci.* **2022**, *13* (29), 8457–8490.
- (8) Wang, Z.; Ivanov, M.; Gao, Y.; Bussotti, L.; Foggi, P.; Zhang, H.; Russo, N.; Dick, B.; Zhao, J.; Di Donato, M.; Mazzone, G.; Luo, L.; Fedin, M. Spin–Orbit Charge–Transfer Intersystem Crossing (ISC) in Compact Electron Donor–Acceptor Dyads: ISC Mechanism and Application as Novel and Potent Photodynamic Therapy Reagents. *Chem. Eur. J.* **2020**, *26* (5), 1091–1102.
- (9) Ponseca, C. S.; Chábera, P.; Uhlig, J.; Persson, P.; Sundström, V. Ultrafast Electron Dynamics in Solar Energy Conversion. *Chem. Rev.* **2017**, *117* (16), 10940–11024.
- (10) Arunkumar, S.; Ghosh, D.; Kumar, G. R. Heavy Main Group Element Containing Organometallic Phosphorescent Materials. *Results Chem.* **2022**, *4*, No. 100399.
- (11) Sasaki, Y.; Yanai, N.; Kimizuka, N. Osmium Complex–Chromophore Conjugates with Both Singlet-to-Triplet Absorption and Long Triplet Lifetime through Tuning of the Heavy-Atom Effect. *Inorg. Chem.* **2022**, *61* (16), 5982–5990.
- (12) Baková, R.; Chergui, M.; Daniel, C.; Vlček, A., Jr.; Zálšíš, S. Relativistic effects in spectroscopy and photophysics of heavy-metal complexes illustrated by spin–orbit calculations of [Re(Imidazole)–(CO)<sub>3</sub>(Phen)]<sup>+</sup>. *Coord. Chem. Rev.* **2011**, *255* (7–8), 975–989.
- (13) Imran, M.; Zhang, X.; Wang, Z.; Chen, X.; Zhao, J.; Barbon, A.; Voronkova, V. K. Electron spin dynamics in excited state photochemistry: recent development in the study of intersystem crossing and charge transfer in organic compounds. *Phys. Chem. Chem. Phys.* **2021**, *23* (30), 15835–15868.
- (14) Baba, M. Intersystem Crossing in the <sup>1</sup>nπ\* and <sup>1</sup>ππ\* States. *J. Phys. Chem. A* **2011**, *115* (34), 9514–9519.
- (15) Zhao, J.; Chen, K.; Hou, Y.; Che, Y.; Liu, L.; Jia, D. Recent progress in heavy atom-free organic compounds showing unexpected intersystem crossing (ISC) ability. *Org. Biomol. Chem.* **2018**, *16* (20), 3692–3701.
- (16) Penfold, T. J.; Gindensperger, E.; Daniel, C.; Marian, C. M. Spin-Vibronic Mechanism for Intersystem Crossing. *Chem. Rev.* **2018**, *118* (15), 6975–7025.
- (17) Marian, C. M. Spin–orbit coupling and intersystem crossing in molecules. *WIREs Comput. Mol. Sci.* **2012**, *2* (2), 187–203.
- (18) Marian, C. M. Understanding and controlling intersystem crossing in molecules. *Annu. Rev. Phys. Chem.* **2021**, *72* (1), 617–640.
- (19) Anders Borg, O. A singlet mechanism for photodissociation of bromofluorobenzenes. *Chem. Phys. Lett.* **2007**, *436* (1–3), 57–62.
- (20) Chen, S.-F.; Liu, F.-Y.; Liu, Y.-J. An *ab initio* investigation of the mechanisms of photodissociation in bromobenzene and iodobenzene. *J. Chem. Phys.* **2009**, *131* (12), No. 124304.
- (21) Rublev, P.; Boldyrev, A. I.; Scheiner, S. Analysis of the Ability of C<sub>6</sub>H<sub>5</sub>I to Phosphoresce. *J. Phys. Chem. A* **2023**, *127* (23), 4927–4933.
- (22) Drescher, L.; Galbraith, M. C. E.; Reitsma, G.; Dura, J.; Zhavoronkov, N.; Patchkovskii, S.; Vrakking, M. J. J.; Mikosch, J. Communication: XUV transient absorption spectroscopy of iodomethane and iodobenzene photodissociation. *J. Chem. Phys.* **2016**, *145* (1), No. 011101.
- (23) Sobolewski, A. L.; Domcke, W. Conical intersections induced by repulsive <sup>1</sup>πσ\* states in planar organic molecules: malonaldehyde, pyrrole and chlorobenzene as photochemical model systems. *Chem. Phys.* **2000**, *259* (2–3), 181–191.
- (24) Hwang, H. J.; El-Sayed, M. A. Determination of the rapid energy redistribution in a transition state by using molecular rotation as a clock and translational energy release as an energy monitor: The photodissociation of iodobenzene. *J. Chem. Phys.* **1992**, *96* (1), 856–858.
- (25) Weike, N.; Chanut, E.; Hoppe, H.; Eisfeld, W. Development of a fully coupled diabatic spin–orbit model for the photodissociation of phenyl iodide. *J. Chem. Phys.* **2022**, *156* (22), No. 224109.
- (26) Zhang, X.; Wei, Z.; Tang, Y.; Chao, T.; Zhang, B.; Lin, K. Halogen Effect on the Photodissociation Mechanism for Gas-Phase Bromobenzene and Iodobenzene. *ChemPhysChem* **2008**, *9* (8), 1130–1136.
- (27) Cheng, P. Y.; Zhong, D.; Zewail, A. H. Kinetic-energy, femtosecond resolved reaction dynamics. Modes of dissociation (in iodobenzene) from time-velocity correlations. *Chem. Phys. Lett.* **1995**, *237* (5–6), 399–405.
- (28) Liu, Y.-J.; Persson, P.; Lunell, S. Multireference calculations of the phosphorescence and photodissociation of chlorobenzene. *J. Chem. Phys.* **2004**, *121* (22), 11000–11006.
- (29) Sage, A. G.; Oliver, T. A. A.; Murdock, D.; Crow, M. B.; Ritchie, G. A. D.; Harvey, J. N.; Ashfold, M. N. R. nσ\* and πσ\* excited states in aryl halide photochemistry: a comprehensive study of the UV photodissociation dynamics of iodobenzene. *Phys. Chem. Chem. Phys.* **2011**, *13* (18), 8075.

- (30) Hwang, H. J.; El-Sayed, M. A. Photodissociation dynamics of iodobenzene by state-selective photofragment translational spectroscopy. *J. Photochem. Photobiol. Chem.* **1996**, *102* (1), 13–20.
- (31) Freedman, A.; Yang, S. C.; Kawasaki, M.; Bersohn, R. Photodissociation of aryl and aryl–alkyl Halides at 193 nm: Fragment translational energy distributions. *J. Chem. Phys.* **1980**, *72* (2), 1028–1033.
- (32) Kadi, M.; Davidsson, J.; Tarnovsky, A. N.; Rasmusson, M.; Åkesson, E. Photodissociation of aryl halides in the gas phase studied with femtosecond pump-probe spectroscopy. *Chem. Phys. Lett.* **2001**, *350* (1–2), 93–98.
- (33) Rasmusson, M.; Lindh, R.; Lascoux, N.; Tarnovsky, A. N.; Kadi, M.; Kühn, O.; Sundström, V.; Åkesson, E. Photodissociation of bromobenzene in solution. *Chem. Phys. Lett.* **2003**, *367* (5–6), 759–766.
- (34) Kavita, K.; Das, P. K. Photodissociation of  $C_6H_5I$ ,  $C_6F_5I$ , and related iodides in the ultraviolet. *J. Chem. Phys.* **2002**, *117* (5), 2038–2044.
- (35) Wolf, W.; Kharasch, N. Photolysis of Iodoaromatic Compounds in Benzene<sup>1</sup>. *J. Org. Chem.* **1965**, *30* (8), 2493–2498.
- (36) Devarajan, A.; Gaenko, A.; Lindh, R.; Malmqvist, P. Role of electronic curve crossing of benzene  $S_1$  state in the photodissociation of aryl halides, effect of fluorination: RASSI-SO MS-CASPT2 Study. *Int. J. Quantum Chem.* **2009**, *109* (9), 1962–1974.
- (37) Liu, Y.-J.; Persson, P.; Lunell, S. Theoretical Study of the Fast Photodissociation Channels of the Monohalobenzenes. *J. Phys. Chem. A* **2004**, *108* (12), 2339–2345.
- (38) Stankus, B.; Zotev, N.; Rogers, D. M.; Gao, Y.; Odate, A.; Kirrander, A.; Weber, P. M. Ultrafast photodissociation dynamics of 1,4-diiodobenzene. *J. Chem. Phys.* **2018**, *148* (19), No. 194306.
- (39) Hu, C.; Tang, Y.; Song, X.; Liu, Z.; Zhang, B. Ultrafast Photodissociation Dynamics of Highly Excited Iodobenzene on the C Band. *J. Phys. Chem. A* **2016**, *120* (51), 10088–10095.
- (40) Mai, S.; Marquetand, P.; González, L. Nonadiabatic dynamics: The SHARC Approach. *WIREs Comput. Mol. Sci.* **2018**, *8* (6), No. e1370.
- (41) Mai, S.; Avagliano, D.; Heindl, M.; Marquetand, P.; Menger, M. F. S. J.; Oppel, M.; Plasser, F.; Polonius, S.; Ruckebauer, M.; Shu, Y.; Truhlar, D. G.; Zhang, L.; Zobel, P.; González, L. SHARC3.0: Surface Hopping Including Arbitrary Couplings—Program Package for Non-Adiabatic Dynamics. *Zenodo* 2023. DOI: 10.5281/ZENODO.7828641.
- (42) Zanchet, A.; Roncero, O.; Karabulut, E.; Solem, N.; Romanzin, C.; Thissen, R.; Alcaraz, C. The role of intersystem crossing in the reactive collision of  $S^+(^4S)$  with  $H_2$ . *J. Chem. Phys.* **2024**, *161* (4), No. 044302.
- (43) Shiozaki, T.; Györfy, W.; Celani, P.; Werner, H.-J. Communication: Extended multi-state complete active space second-order perturbation theory: Energy and nuclear gradients. *J. Chem. Phys.* **2011**, *135* (8), No. 081106.
- (44) Granovsky, A. A. Extended multi-configuration quasi-degenerate perturbation theory: The new approach to multi-state multi-reference perturbation theory. *J. Chem. Phys.* **2011**, *134* (21), No. 214113.
- (45) Widmark, P.-O.; Malmqvist, P. Å.; Roos, B. O. Density matrix averaged atomic natural orbital (ANO) basis sets for correlated molecular wave functions: I. First row atoms. *Theor. Chim. Acta* **1990**, *77* (5), 291–306.
- (46) Forsberg, N.; Malmqvist, P.-Å. Multiconfiguration perturbation theory with imaginary level shift. *Chem. Phys. Lett.* **1997**, *274* (1–3), 196–204.
- (47) Reiher, M. Douglas–Kroll–Hess Theory: a relativistic electrons-only theory for chemistry. *Theor. Chem. Acc.* **2006**, *116* (1–3), 241–252.
- (48) Malmqvist, P. Å.; Roos, B. O.; Schimmelpfennig, B. The restricted active space (RAS) state interaction approach with spin-orbit coupling. *Chem. Phys. Lett.* **2002**, *357* (3–4), 230–240.
- (49) Aquilante, F.; Autschbach, J.; Baiardi, A.; Battaglia, S.; Borin, V. A.; Chibotaru, L. F.; Conti, I.; De Vico, L.; Delcey, M.; Fdez. Galván, I.; Ferré, N.; Freitag, L.; Garavelli, M.; Gong, X.; Knecht, S.; Larsson, E. D.; Lindh, R.; Lundberg, M.; Malmqvist, P. Å.; Nenov, A.; Norell, J.; Odelius, M.; Olivucci, M.; Pedersen, T. B.; Pedraza-González, L.; Phung, Q. M.; Pierloot, K.; Reiher, M.; Schapiro, I.; Segarra-Martí, J.; Segatta, F.; Seijo, L.; Sen, S.; Sergentu, D.-C.; Stein, C. J.; Ungur, L.; Vacher, M.; Valentini, A.; Velyazov, V. Modern quantum chemistry with [Open]Molcas. *J. Chem. Phys.* **2020**, *152* (21), No. 214117.
- (50) Fdez. Galván, I.; Vacher, M.; Alavi, A.; Angeli, C.; Aquilante, F.; Autschbach, J.; Bao, J. J.; Bokarev, S. I.; Bogdanov, N. A.; Carlson, R. K.; Chibotaru, L. F.; Creutzberg, J.; Dattani, N.; Delcey, M. G.; Dong, S. S.; Dreuw, A.; Freitag, L.; Frutos, L. M.; Gagliardi, L.; Gendron, F.; Giussani, A.; González, L.; Grell, G.; Guo, M.; Hoyer, C. E.; Johansson, M.; Keller, S.; Knecht, S.; Kováčević, G.; Källman, E.; Li Manni, G.; Lundberg, M.; Ma, Y.; Mai, S.; Malhado, J. P.; Malmqvist, P. Å.; Marquetand, P.; Mewes, S. A.; Norell, J.; Olivucci, M.; Oppel, M.; Phung, Q. M.; Pierloot, K.; Plasser, F.; Reiher, M.; Sand, A. M.; Schapiro, I.; Sharma, P.; Stein, C. J.; Sørensen, L. K.; Truhlar, D. G.; Ugandi, M.; Ungur, L.; Valentini, A.; Vancollie, S.; Velyazov, V.; Weser, O.; Wesolowski, T. A.; Widmark, P.-O.; Wouters, S.; Zech, A.; Zobel, J. P.; Lindh, R. OpenMolcas: From Source Code to Insight. *J. Chem. Theory Comput.* **2019**, *15* (11), 5925–5964.
- (51) Li Manni, G.; Fdez. Galván, I.; Alavi, A.; Aleotti, F.; Aquilante, F.; Autschbach, J.; Avagliano, D.; Baiardi, A.; Bao, J. J.; Battaglia, S.; Birnoschi, L.; Blanco-González, A.; Bokarev, S. I.; Broer, R.; Cacciari, R.; Calio, P. B.; Carlson, R. K.; Carvalho Couto, R.; Cerdán, L.; Chibotaru, L. F.; Chilton, N. F.; Church, J. R.; Conti, I.; Coriani, S.; Cuéllar-Zuquin, J.; Daoud, R. E.; Dattani, N.; Decleva, P.; De Graaf, C.; Delcey, M. G.; De Vico, L.; Dobrautz, W.; Dong, S. S.; Feng, R.; Ferré, N.; Filatov Gulak, M.; Gagliardi, L.; Garavelli, M.; González, L.; Guan, Y.; Guo, M.; Hennefarth, M. R.; Hermes, M. R.; Hoyer, C. E.; Huix-Rotllant, M.; Jaiswal, V. K.; Kaiser, A.; Kaliaikin, D. S.; Khamesian, M.; King, D. S.; Kochetov, V.; Krošnicki, M.; Kumar, A. A.; Larsson, E. D.; Lehtola, S.; Lepetit, M.-B.; Lischka, H.; López Ríos, P.; Lundberg, M.; Ma, D.; Mai, S.; Marquetand, P.; Merritt, I. C. D.; Montorsi, F.; Mörchen, M.; Nenov, A.; Nguyen, V. H. A.; Nishimoto, Y.; Oakley, M. S.; Olivucci, M.; Oppel, M.; Padula, D.; Pandharkar, R.; Phung, Q. M.; Plasser, F.; Raggi, G.; Rebolini, E.; Reiher, M.; Rivalta, I.; Roca-Sanjuán, D.; Romig, T.; Safari, A. A.; Sánchez-Mansilla, A.; Sand, A. M.; Schapiro, I.; Scott, T. R.; Segarra-Martí, J.; Segatta, F.; Sergentu, D.-C.; Sharma, P.; Shepard, R.; Shu, Y.; Staab, J. K.; Straatsma, T. P.; Sørensen, L. K.; Tenorio, B. N. C.; Truhlar, D. G.; Ungur, L.; Vacher, M.; Velyazov, V.; Voß, T. A.; Weser, O.; Wu, D.; Yang, X.; Yarkony, D.; Zhou, C.; Zobel, J. P.; Lindh, R. The OpenMolcas Web: A Community-Driven Approach to Advancing Computational Chemistry. *J. Chem. Theory Comput.* **2023**, *19* (20), 6933–6991.
- (52) Heß, B. A.; Marian, C. M.; Wahlgren, U.; Gropen, O. A mean-field spin-orbit method applicable to correlated wavefunctions. *Chem. Phys. Lett.* **1996**, *251* (5–6), 365–371.
- (53) Aquilante, F.; Lindh, R.; Bondo Pedersen, T. Unbiased auxiliary basis sets for accurate two-electron integral approximations. *J. Chem. Phys.* **2007**, *127* (11), No. 114107.
- (54) Granucci, G.; Persico, M. Critical appraisal of the fewest switches algorithm for surface hopping. *J. Chem. Phys.* **2007**, *126* (13), No. 134114.
- (55) Plasser, F.; Ruckebauer, M.; Mai, S.; Oppel, M.; Marquetand, P.; González, L. Efficient and Flexible Computation of Many-Electron Wave Function Overlaps. *J. Chem. Theory Comput.* **2016**, *12* (3), 1207–1219.
- (56) Plasser, F.; Barbatti, M.; Aquino, A. J. A.; Lischka, H. Excited-State Diproton Transfer in [2,2'-Bipyridyl]-3,3'-Diol: The Mechanism Is Sequential Not Concerted. *J. Phys. Chem. A* **2009**, *113* (30), 8490–8499.
- (57) Granucci, G.; Persico, M.; Zocante, A. Including quantum decoherence in surface hopping. *J. Chem. Phys.* **2010**, *133* (13), No. 134111.